# Anisotropic Scattering of the Radio Emission in the Direction to Pulsar B1642—03

# M. V. Popov\*

Astro Space Center, Physical Institute, Russian Academy of Sciences, Moscow, 117997 Russia
\*e-mail: popov069@asc.rssi.ru

Received September 4, 2024; revised October 20, 2024; accepted November 11, 2024

Abstract—Pulsar B1642-03 has been observed with the Radioastron ground-space interferometer during the implementation of the Key Science Program of the project. Observations were made on September 8, 2013, in the 92-cm band at frequencies 316-332 MHz. The Westerbork Synthesis RT (WSRT) has been used as a ground arm of the interferometer. The baseline projections of the interferometer have changed during the observations approximately from 10000 to 20000 km, and the positional angle of the baseline has changed almost for  $50^{\circ}$ . This configuration has made it possible to estimate the angular diameter of the scattering disk in different positional angles. It has been found that the shape of the scattering disk can be presented in the form of an ellipse with an axial ratio of 2: 1. Comparison of the angular size of the scattering disk and the delay time of scattered rays has indicated a possible irregular structure of the scattering disk, which may be due to lensing of radio waves when passing through the Stromgren zone near star  $\zeta$  Oph.

**Keywords:** pulsar B1642–03, very long baseline interferometry, interstellar scattering

**DOI:** 10.1134/S1063772925701513

#### 1. INTRODUCTION

In 2011, the Russian Academy of Sciences and the Federal Space Agency created an orbital space observatory with a 10 meter radio telescope, which, when working together with a ground-based network of radio telescopes, formed the RadioAstron ground-space interferometer. The space radio telescope revolved around the Earth in an elongated elliptical orbit with an apogee distance of 350000 km, which made it possible to increase the resolution of the ground-space interferometer by 25 times compared to a purely ground-based VLBI network. Over seven years of work, many new and unique scientific results were obtained [1].

The 316–332 MHz frequency range was used for observing pulsars. The angular dimensions of the region of radio emission of a pulsar located in the magnetosphere of a neutron star are extremely small and are certainly less than an angular microsecond. Such dimensions are unresolved even with a ground-space interferometer. However, as a result of interstellar scattering, the pulsar's image appears as a "scattering disk" with characteristic angular size  $\theta_{\rm scat}$ , which falls in the range of milliarcseconds (mas). Such angular dimensions are effectively measured by the Radio-Astron ground-space interferometer, which has a maximal resolution of 0.5 mas in the range of 316–332 MHz.

As a result of the analysis of the scattering effects with such a high angular and temporal resolution, a number of effects and features, such as the substructure of the scattering disk [2, 3] and anisotropic scattering in the direction of the Vela pulsar [4] and in the direction of the B0834+06 pulsar [5], were discovered.

This study is aimed to measure the shape of the scattering disk in the direction of pulsar B1642–03 by analyzing observations with the RadioAstron ground-space interferometer.

## 2. CHARACTERISTICS OF OBSERVATIONAL DATA

In this study, we used observations of pulsar B1642–03 carried out with the RadioAstron ground-space interferometer during the implementation of the Key Science Program of the project. The observations were conducted on September 8, 2013, in the 92-cm band (316–332 MHz) for two hours in a configuration with the Space Radio Telescope (SRT) and the Westerbork Aperture Synthesis Telescope (WSRT) as the ground arm of the interferometer (GRT). Reception of radio emission was carried out in two polarization channels with left (LCP) and right (RCP) circular polarizations. Data recording was performed in 570-s scans with 30 s breaks. On the space telescope, signal registration was performed with two-level quantization, while on the ground-based telescope, four-level

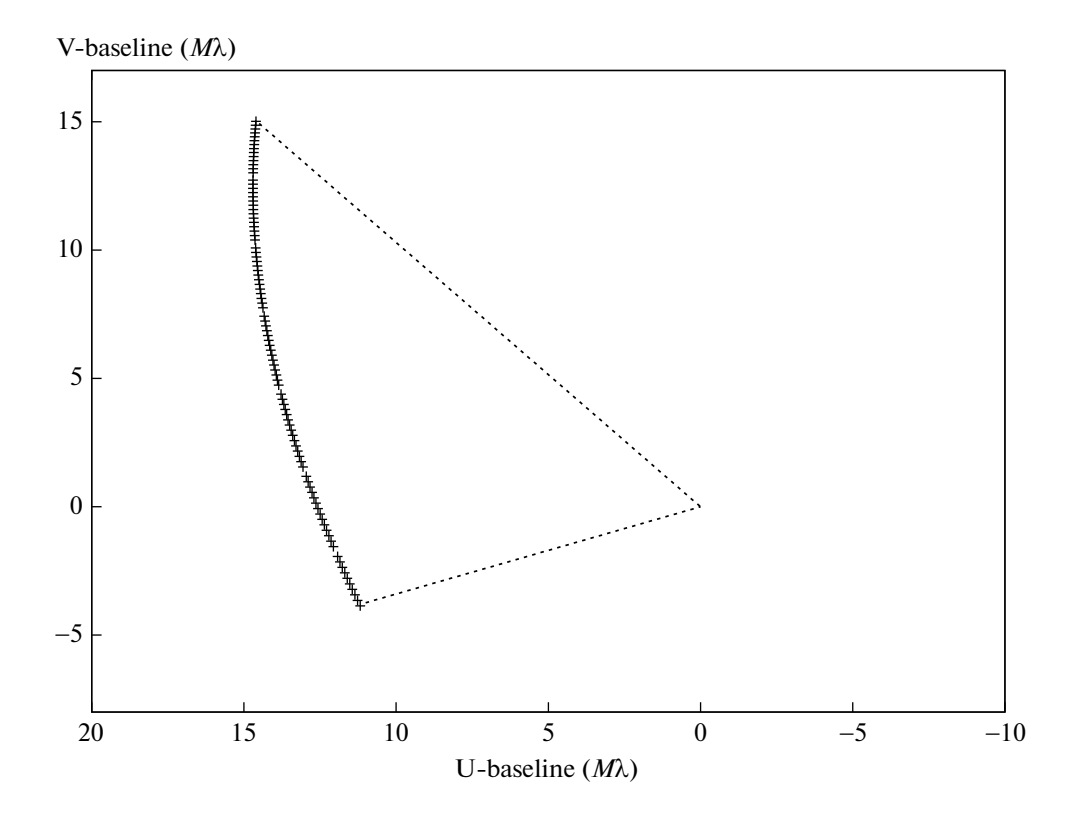


Fig. 1. Change in the baseline projection of the ground-space interferometer during the observation period. The used  $M\lambda$  unit of length is expressed in millions of wavelengths.

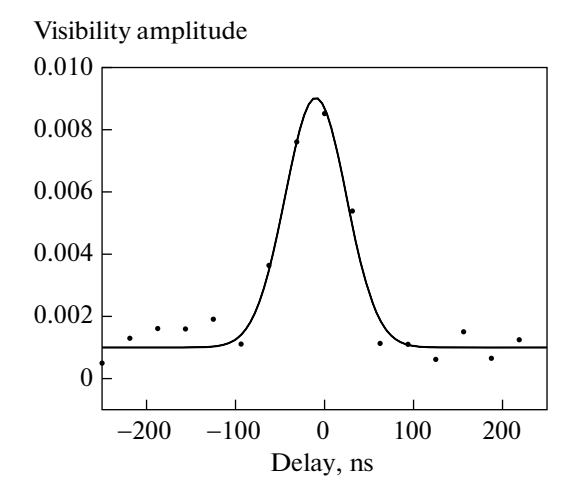
quantization was used. During one hour of total observation time, 9760 pulses of the pulsar were recorded; the pulse repetition period of this pulsar is 0.3876 s. The data correlation was carried out on the correlator of the Astrospace Center FIAN [6] using a pulse "window" (on) and with compensation for the influence of radio wave dispersion. For calibration purposes, correlation of data outside the pulse window of the same duration (off) was also performed. The correlation used 8192 spectral channels, which provides a frequency resolution of 1.95 kHz.

Figure 1 shows the change in the projection of the base of the ground-space interferometer during the observation period. The used  $M\lambda$  unit of length is expressed in millions of wavelengths. Wavelength  $\lambda$ , on which the observations were made, is equal to 92 cm. The magnitude of the base projection changed approximately twofold, from 10000 to 20000 km, and the position angle of the base projection changed by almost 50°. This configuration opens up good prospects for analyzing the shape of the scattering disk.

## 3. VISIBILITY FUNCTION AMPLITUDE

A fundamental quantity in interferometric measurements is the visibility function,  $\tilde{V}_{ab}(v,t) = \tilde{E}_a(v,t)\tilde{E}_b^*(v,t)$ , which is the product of the electric

fields (voltage) recorded by radio telescopes "a" and "b." The correlator produces this value and averages the  $\tilde{V}_{ab}(v,t)$  complex values over the duration of the pulse window in the case of pulsar observations, while the  $\Delta t$  time step of the data output by the correlator is equal to the p pulse repetition period of the pulsar. Frequency step  $\Delta v$  is determined by the selected  $N_{\rm ch}$ number of channels. Function  $\tilde{V}_{ab}(v,t)$  in most cases is called a cross-spectrum. Inverse Fourier transform of cross spectrum  $\tilde{V}_{ab}(v,t)$  provides visibility function  $\tilde{V}_{ab}(\tau,t)$  depending on signal delay  $\tau$  between telescopes; in fact, this is a cross-correlation function of the field recorded by these telescopes. This value is analyzed when constructing a radio image of the studied objects. To determine correctly the amplitude of the visibility function, the Fourier transform over time of a set of functions  $\tilde{V}_{ab}(\tau,t)$  is used on time interval  $T_{\rm int}$ , which gives visibility function  $\tilde{V}_{\rm ab}(\tau,f)$  in the coordinates of "delay"  $\tau$  and "fringe rate" f, which in the ideal case has a maximum amplitude at  $\tau = 0$ and f = 0. This representation of the visibility function makes it possible to find the maximal value of the amplitude even with inaccurate knowledge of the clock corrections and the orbital parameters of the spacecraft when this maximum turns out to be shifted and is found at values of  $\tau = \tau_1$  and  $f = f_1$ . The



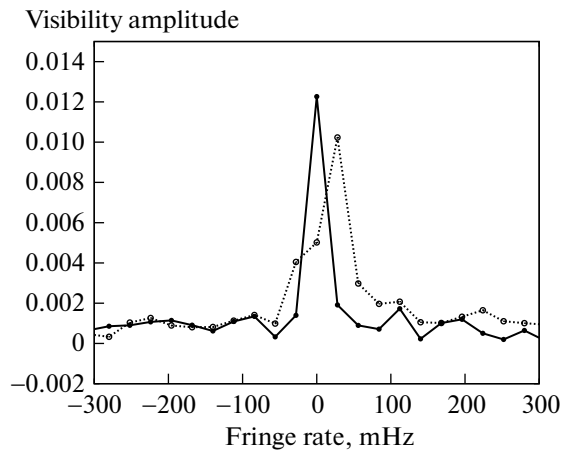


Fig. 2. Sections of the "fringe rate—delay" diagram by delay (left) and by fringe rate (right) for a signal received in a channel with left circular polarization (LCP). The delay time scale (left) is digitized in ns, and the residual fringe rate scale (right) is digitized in mHz. The ordinate axis shows the amplitude of the visibility function without normalization.

shift may also be caused by the influence of radio wave scattering on inhomogeneities in the interstellar plasma or in the Earth's ionosphere.

The correlator of the Astrospace Center of the Lebedev Physical Institute [6] calculates (integrates) cross-spectra  $\tilde{V}_{ab}(v,t)$  when processing pulsars in the "window" of the pulsar pulse radiation and produces a result with a time step equal to the pulse repetition period of p=0.3876 s. The integration window duration in our case was 9 ms.

The dynamic spectrum of pulsar B1642–03 was analyzed in detail by Bartel et al. [7]. They determined the decorrelation bandwidth of  $\Delta v = 930$  kHz and characteristic scintillation time of  $\Delta t_{\rm scint} = 40$  s. To determine the amplitude of the visibility function in our experiment, two-dimensional "fringe rate—delay" diagrams were constructed, representing the behavior of the module of function  $\tilde{V}_{\rm ab}(\tau,f)$ . These diagrams were constructed for each hundred consecutive pulses, so that the integration time is  $T_{\rm int} = 100p = 38.76$  s, which is comparable with the characteristic scintillation time. In these diagrams, delay step  $\tau$  corresponds to the sampling time of  $\delta \tau = 31.25$  ns, while the step in fringe rate is  $\delta f = 1/T_{\rm int} = 25.8$  mHz. A total of 79 such realizations were obtained for this analysis.

Figure 2 shows examples of the cross section of the "fringe rate—delay" diagram by delay (left) and by fringe rate (right) for a signal in a channel with left circular polarization. For the delay section, the calculated values are represented by dots, and the solid line shows the approximation of these values by the Gaussian function on the interval of  $\pm 5$  counts from the maximal position. The amplitude of this approximat-

ing function was taken for the subsequent analysis. Thus, a correction for the fractional part of the reading was made, since the maximum of the function did not fall on the integer values of the delay. It should be noted that this shift did not exceed one count during the entire observation session.

A more complex situation is realized in the fringe rate section. For this cross-section, Fig. 2 provides two examples for two signal samples of 100 pulses each: one sample shown as a solid line passing through the dots demonstrates a cross section as a delta function (we call such a cross section normal); the other sample shown in the figure as a dotted line passing through the circles gives an extended cross section with a reduced amplitude and a maximum shifted by one step (we call this cross section distorted). In our opinion, these distortions are caused by the influence of the ionosphere. Similar ionospheric effects discovered by the Radio-Astron ground-space interferometer were discussed in the study of Popov et al. [8]. These ionospheric effects are broadband in nature and do not affect the shape of the visibility function by delay, but lead to an expansion of the function by interference frequency with a corresponding decrease in amplitude.

To correct the amplitude of the visibility function for these distortions, the  $W_{1/2}$  half-width of the function in the cross section at the fringe rate was calculated by approximation with a Gaussian function on the interval of  $\pm 5$  counts from the maximal position for each time sample. Received  $W_{1/2}(t)$  values show significant variations over time. Figure 3 shows the autocorrelation function (ACF) of the time variations of the  $W_{1/2}(t)$  half-width of the cross section by the fringe rate. It is evident in the figure that the amplitude of ACF oscillations is  $\sim 0.2$  and has a quasi-periodic

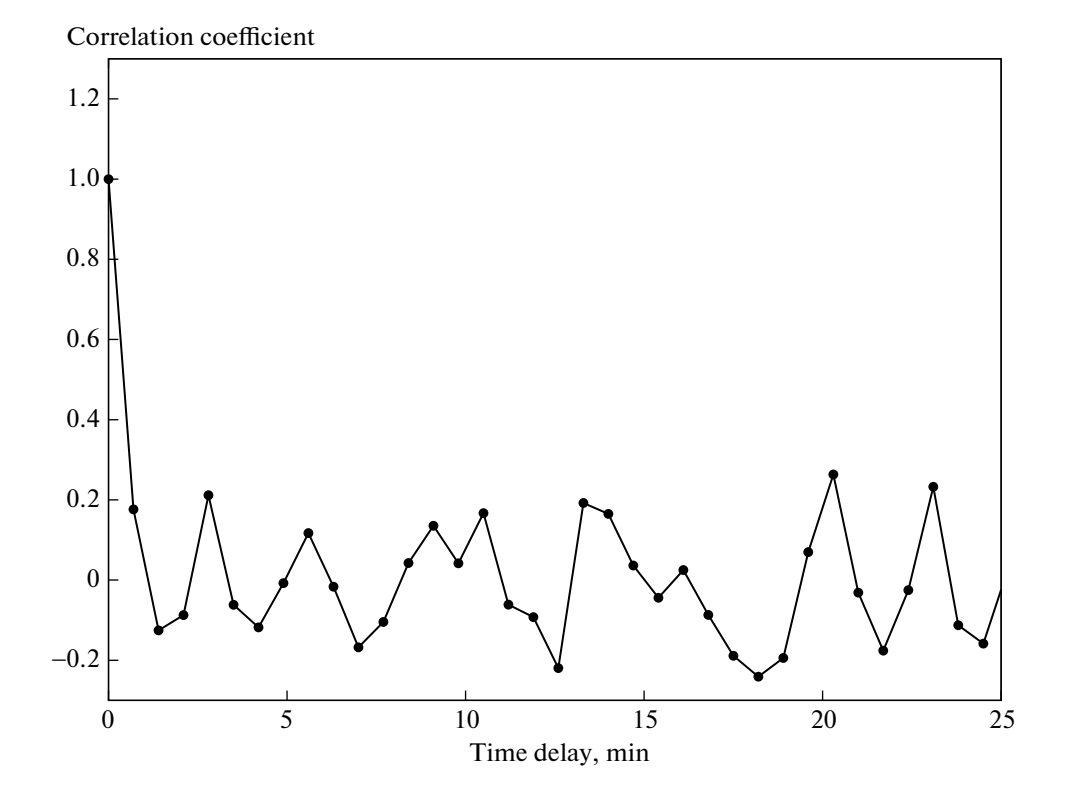


Fig. 3. ACF of variations in the width of the visibility function in the cross section by the fringe rate (polarization channel with LCP). The abscissa axis shows the delay time in min, and the ordinate axis shows the correlation coefficient.

character with a characteristic time of  $\sim 3$  min. Since autocorrelation is a quadratic function, the amplitude of the half-width variations themselves reaches the level of 0.45 of its average value.

If we assume that with ionospheric distortions the area under the curve describing the cross section of the amplitude of the visibility function by the interference frequency is preserved, i.e.,  $S_0 = A_0 W_0 = S_1 = A_1 W_1$ , where  $A_0$  and  $W_0$  are the amplitude and half-width of the function for the "normal" section (solid line in Fig. 2), and  $A_1$  and  $W_1$  are the amplitude and halfwidth of the function for the "distorted" section (dotted line in Fig. 2), then, the corrected amplitude of the visibility function will be obtained from relation  $A_{\text{cor}} = A_i(W_i/W_0)$ . Even from the simple example shown in Fig. 2 on the right, it is clear that this correction produces an incorrect result, namely, the halfwidth of the "distorted" section is at least twice the half-width of the "normal" section, while the amplitude of the "distorted" section is only 1.2 times less than the amplitude of the "normal" section. As a result of a more careful comparison of the cases of "normal" and "distorted" cross-sections, the following ratio was obtained:  $A_{cor} = A_i \sqrt{(W_i/W_0)}$ . This ratio was used to correct the calculated amplitudes of the visibility function. The value corrected for the fractional part of the reading was taken as the  $A_i$  value as was described above.

Next, the values of the visibility function amplitude were normalized so that these values were expressed as fractions of the received radio flux. This normalization takes into account the sensitivities of the participating radio telescopes and the significant variability of the pulsar's own radio flux density. The normalization technique for observing pulsars using a ground-space interferometer was presented in the study of Popov et al. [9]. The normalization coefficient was calculated using the following formula taken from the specified publication:

$$R^{-1} = \left(\frac{\sigma_{SRT}}{\sigma_{GRT}}\right)_{off} (\sigma_{on}^2 - \sigma_{off}^2) \sqrt{\eta}.$$
 (1)

The SRT index refers to a space telescope, and the GRT index refers to a ground-based telescope. Ratio

of root mean square fluctuations  $\left(\frac{\sigma_{SRT}}{\sigma_{GRT}}\right)$  was calculated for the signal outside the pulse window (off). This ratio did not change during the observation period and was 0.465. The difference in signal dispersion in and out of the pulse window was calculated for the WSRT ground-based radio telescope; this value determines the normalization. The average value for

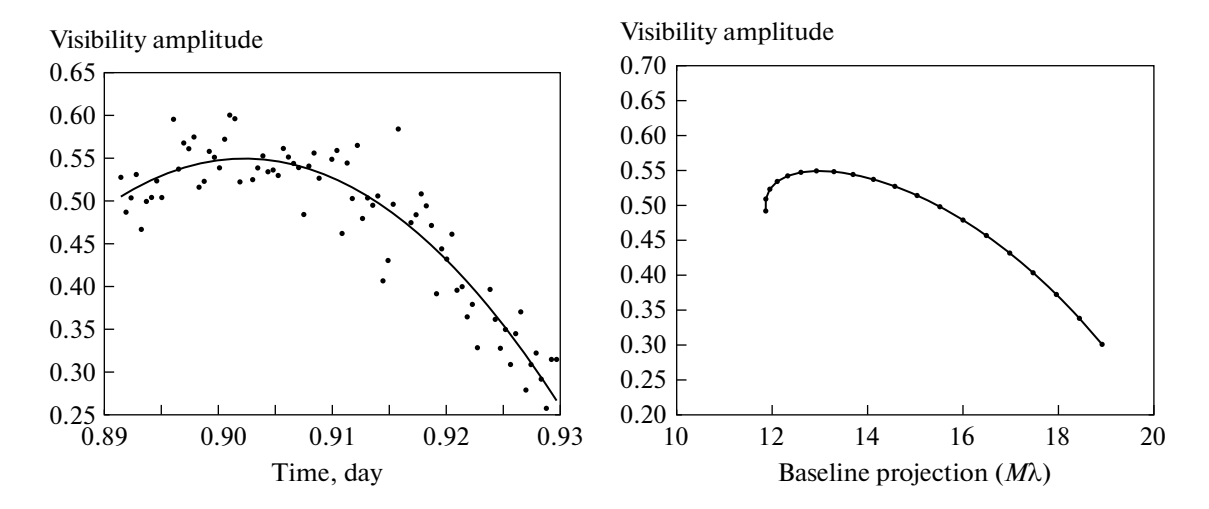


**Fig. 4.** Approximation of the behavior of the visibility function amplitude over time (left) and the dependence of the averaged visibility function amplitude on the baseline projection of the ground-space interferometer (right). The observation time is given in fractions of a day, and the baseline projection is given in millions of wavelengths.

each realisation of one hundred pulses was used. On average, this difference was around 0.5. Coefficient

 $\eta = \frac{SEFD_{SRT}}{SEFD_{GRT}}$  is equal to the ratio of the system temperatures that is expressed in Jansky (system equiva-

peratures that is expressed in Jansky (system equivalent flux density) for space and ground-based radio telescopes. This ratio was determined in the already cited study of Popov et al. [9] based on observations of bright pulsar B0329+54. They provide the value of  $\eta = 0.0063$  obtained with allowance for the loss of sensitivity of the space radio telescope due to two-level quantization of the signal. Taking into account all these coefficients, it turned out that the "raw" values of the visibility function amplitude should be increased by approximately 50 times.

This normalization for two polarization channels was carried out separately. The obtained values were then averaged. These values averaged over the two channels were used in further analysis.

Figure 4 (left) shows the change over time of the normalized and averaged over two channels amplitude of the visibility function. There is a significant variation in individual values. This spread is due to our method of measuring the amplitude of the visibility function on a time interval of  $T_{\rm int} = 100 p = 38.76$  s comparable with the characteristic scintillation time of  $\Delta t_{\rm scint} = 40$  s. Such observing mode is called snap shot mode. In this mode, the visibility function varies in amplitude because of scintillation. The solid line in Fig. 4 shows the approximation of the data by a parabola. The standard deviation of measurements relative to the approximating curve was 0.03. The averaged values are used to analyze the behavior of the visibility function amplitude depending on the magnitude of

the baseline projection of the ground-space interferometer. This dependence is shown in Fig. 4 (on the right).

## 4. SCATTERING DISK PARAMETERS

Gwin et al. [10] showed that for a scattering disk, the amplitude of the visibility function on the base formed by telescopes "a" and "b" depends on the magnitude of the projection of the interferometer base as follows:

$$V_{ab}(\vec{b}) = \exp\left[-\frac{1}{2}\left(\frac{\pi}{\sqrt{2\ln 2}}\frac{\theta_{\rm H}b}{\lambda}\right)^{n-2}\right],\tag{2}$$

where  $V_{\rm ab}$  is the amplitude of the visibility function, b is the baseline projection,  $\lambda$  is the observation wavelength, and  $\theta_{\rm H}$  is the full width of the pulsar's scattering disk at half maximum. Exponent n of the plasma inhomogeneity spectrum was determined for our pulsar in the study of Bartel et al. [7] and turned out to be equal to  $3.97 \pm 0.05$ . In the following calculations, we adopted n = 4.

The dependence of the average amplitude of the visibility function on the magnitude of the baseline projection of the ground-space interferometer shown in Fig. 4 is non-monotonic. This behavior indicates that the shape of the scattering disk is not circular. On the approximating curve, 40 points equally spaced in time were used ( $\delta t = 86.4$  s), and for the every moment the amplitude of the visibility function, the magnitude of the base projection, and the position angle of the base vector are known. For each point, the angular size of the scattering disk in the direction of

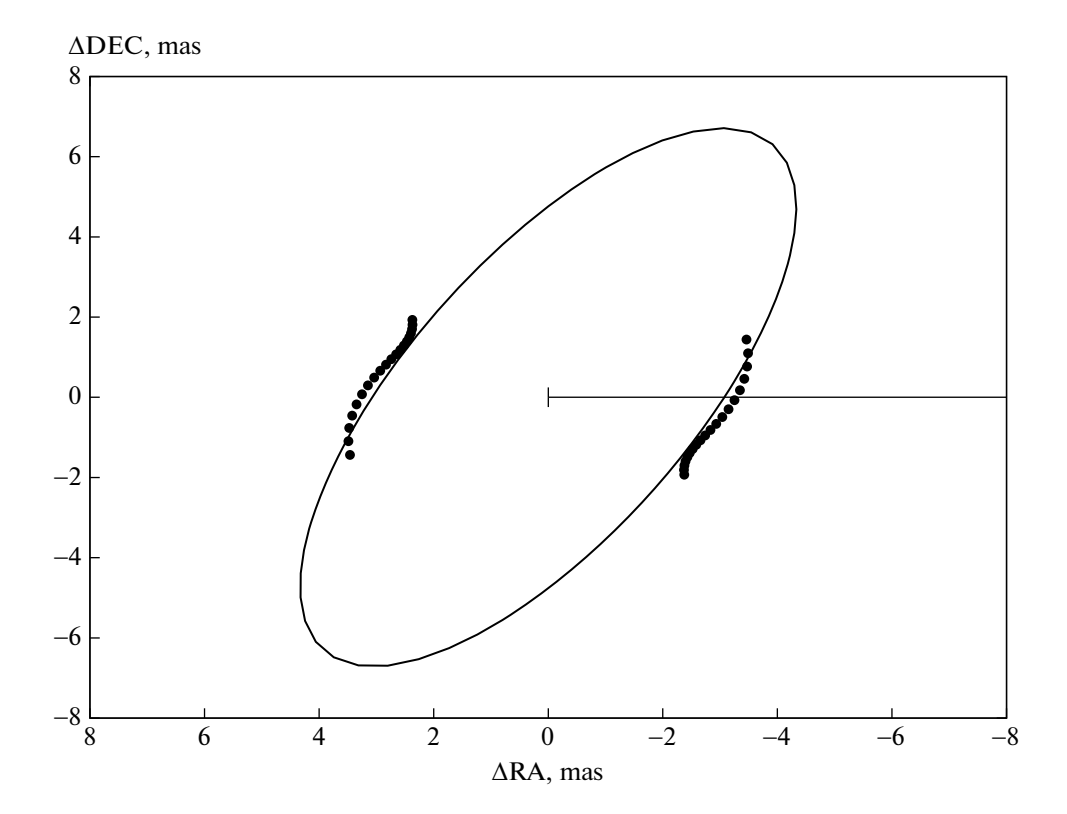


Fig. 5. Approximation of measured values of the scattering disk dimensions for different projections of the interferometer base in the form of an ellipse. The abscissa axis corresponds to right ascension, and the ordinate axis corresponds to declination. The scale of the figure is expressed in milliarcseconds (mas).

the position angle of the base projection was calculated using the formula:

$$\theta_{\rm H} = \frac{0.528}{B} \sqrt{\ln(1/V_{\rm ab})}.$$
 (3)

This expression is obtained from (2) by inversion with respect to  $\theta_{\rm H}$  and after substituting the numerical coefficients. Here,  $B = b/\lambda$  is the magnitude of the base projection, that is expressed in wavelengths, and angle  $\theta_{\rm H}$  is obtained in radians.

Results of calculation of  $\theta_H$  angular sizes of the scattering disk depending on the position angle are represented by dots in Fig. 5. The solid line in this figure shows the result of approximating the measurements with an ellipse function. The following parameters of such an ellipse were obtained: the major axis is  $10.8 \pm 0.5$  mas, the minor axis is  $5.8 \pm 0.04$  mas, and the position angle of the major axis is  $-27.5^{\circ} \pm 1.0^{\circ}$ ; the ratio of the axes of the ellipse is approximately 2:1.

## 5. DISCUSSION

Deller et al. [11] determined the parallax and proper motion of pulsar B1642–03: it is located at a distance of 4 kpc from the Sun and moves with a tan-

gential velocity of ~400 km/s. The galactic coordinates of the pulsar are:  $l = 14^{\circ}$  and  $b = 26^{\circ}$ , and the dispersion measure is  $DM = 35.8 \text{ pc/cm}^3$ . At approximately an angular distance of 8° from the direction to the pulsar, giant star  $\zeta$  Oph of spectral class O9.5 was found at a distance of 140 pc, creating a vast zone of ionized hydrogen H II with a Strömgren radius of ~50 pc [12], covering a region on the sky with a diameter of almost 50°. Thus, the line of sight from the observer to the pulsar completely crosses the Strömgren zone of  $\zeta$  Oph. Star  $\zeta$  Oph itself is a runaway star [13, 14]; it moves at high velocity relative to its surroundings and forms emission nebula Sh2-27 at the base of its outflowing atmosphere as a result of the action of a shock wave. This nebula has an irregular shape with angular dimensions of  $\sim 10^{\circ}$  [15]. The line of sight from the observer to the pulsar passes near the boundary of this

In a special study [16], Pynzar examined the possible influence of the Sh2-27 nebula on the effects of scattering of radio emission from pulsar B1642–03 and concluded that this nebula makes a relatively small contribution to the dispersion measure of the pulsar and to the magnitude of the scattering angle. However, we believe that precisely, the anisotropic scattering by

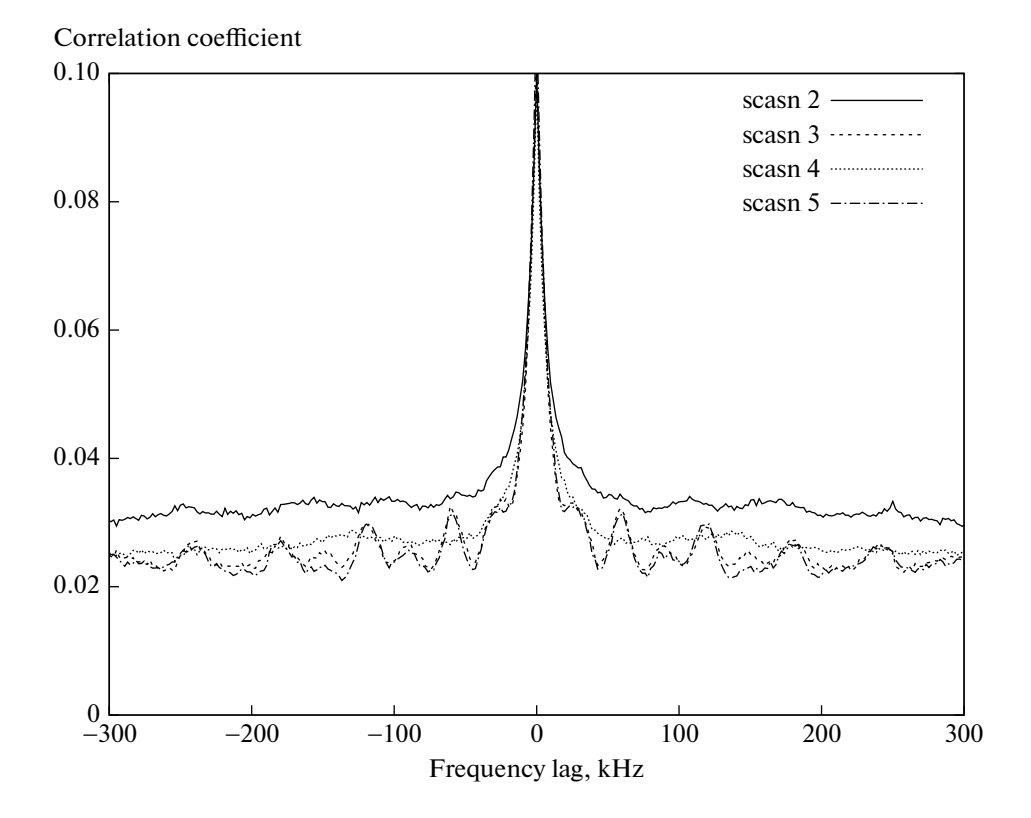


**Fig. 6.** Frequency cross-sections of two-dimensional autocorrelation functions from dynamic spectra for several scans. The frequency shift is given in kHz. The presence of repeating quasi-periodic structures indicates their instrumental origin.

plasma inhomogeneities in the spurs of the Sh2-27 nebula causes the elliptical shape of the scattering disk.

Popov et al. [4] presented an analysis of VLBI observations of pulsar B0833-45. Based on the behavior of the amplitude of the visibility function at different orientations of the base projection, a conclusion about the ellipticity of the scattering disk with an axial ratio of 2:1 was made. Pulsar B0833–45 is located in a supernova remnant in the Vela constellation; the authors of [4] suggested that anisotropic scattering occurs on the shell of the supernova remnant since the position of the scattering screen that is determined from a comparison of scattering angle  $\theta_{\rm H}$  and scattering time  $\tau_{sc}$  was in satisfactory agreement with the position of the boundary of the supernova remnant shell. In the discussed study [4], the relation between  $\theta_H$  and  $\tau_{sc}$ , by which the distance to the scattering screen in the thin screen model can be estimated, is given. We rewrite this relation here in a modified form:

$$\frac{D}{d} = \frac{\theta_{\rm H}^2 D}{8 \ln 2c \tau_{\rm sc}} + 1,\tag{4}$$

where D is the distance to the pulsar, d is the distance from the observer to the screen, and c is the speed of light.

Characteristic scattering time  $\tau_{sc}$  was determined by approximating the delay cross sections with Gaussian functions (see Section 3); an example of this approximation is shown in Fig. 2. The average value was obtained to be  $\tau_{sc}=40\pm2$  ns. Comparison of the values of  $\langle \theta_H \rangle \approx 8.5$  ms and scattering time of  $\tau_{sc} =$ 40 ns we obtained using expression (4) produces the ratio of  $D/d \approx 3000$ . It turns out that in the model of a thin scattering screen, this screen is located at a distance of 1.5-2.5 pc from the observer. This result seems implausible to us and only indicates that the thin screen model in our case does not work. Indeed, the line of sight from the observer to the pulsar crosses the star's Strömgren zone of  $\zeta$  Oph with increased electron density. This zone acts as a diverging lens and increases the scattering angle. The effects of lensing of pulsar radio emission by inhomogeneities of interstellar plasma have been considered in many publications [17–19]. These refractive effects result in the appearance of multiple images of the scatter disk and/or deformation of the scatter disk. In particular, for a regular lens located directly on the line of sight, the scattering disk can take on a quasi-ring structure, for which the delays between the scattered rays turn out to be small even for a large diameter of the scattering disk.

Gwinn et al. [20] conducted VLBI observations of several pulsars at 327 MHz using a ground-based network of radio telescopes with intercontinental bases. Our pulsar B1642–03 was also among the objects of study. The diameter of the scattering disk of  $\theta_{\rm H}=6.7\pm1.1$  mas was measured for it. This finding agrees well with our measurements. However, the value for the  $\Delta v$  decorrelation band given in [20] is only 15 kHz compared to the value we adopted of  $\Delta v=930$  kHz [7]. Accordingly, scattering time  $\tau_{\rm sc}$  in [20] is taken to be equal to 4  $\mu s$  (a hundred times greater than our value).

As was mentioned above, the dynamic spectrum of pulsar B1642-03 was studied in detail for the same observing session in [7]. In this study, it was noted that in addition to the diffraction structure with a decorrelation band of 930 kHz, the spectrum also contains a strange narrow feature with a characteristic band of less than 10 kHz. In this paper, we studied this narrowband structure more thoroughly using higher frequency resolution with a number of channels of  $N_{\rm ch}=8192$  (compared to  $N_{\rm ch}=512$  in [7]). Figure 6 shows the frequency cross sections of the two-dimensional autocorrelation functions from dynamic autospectra at the Westerbork radio telescope for several observation scans. Some ACF scans clearly show similar quasi-periodic structures, indicating their artificial origin. The characteristic frequency width of these structures is ~10 kHz. These manifestations may be caused by resonant standing waves in the feed system or in the diagram synthesis system of the WSRT multielement radio telescope.

## 6. CONCLUSIONS

An analysis of the behavior of the amplitude of the visibility function depending on the magnitude of the baseline projection of the ground-space interferometer indicates that the scattering disk of radio emission from pulsar B1642-03 differs from the circular shape and can be represented as an ellipse with angular dimensions of the axes of  $10.8 \times 5.8$  mas; the position angle of the major axis of the ellipse is  $-27.5^{\circ}$ .

Comparison of the scattering angle values we obtained of  $\langle \theta_H \rangle \approx 8.5$  mas and scattering time of  $\tau_{sc} = 40$  ns indicates that the scattering disk may have a non-uniform structure with concentration towards the edges of the disk. This structure can produce small relative delays of rays with a significant total scattering angle measured by the interferometer. For example, at a hypothetical purely annular shape of the scattering disk, the delay of all scattered rays would be the same, i.e.,  $\tau_{sc} \approx 0$  (excluding the thickness of the ring), while the size of the scattering disk measured by the interferometer may be large.

In our opinion, the features of the scattering of radio emission from pulsar B1642-03 are caused by the influence of nebula Sh2-27 and the H II zone of the  $\zeta$  Oph star of spectral type O9.5 located close to the direction of the pulsar.

A two-element interferometer does make it possible to study the complex structure of the scattering disk. The interesting features of the scattering disk structure that have been discovered can be studied more closely using the global VLBI network of radio telescopes.

#### **FUNDING**

This work was supported by ongoing institutional funding. No additional grants to carry out or direct this particular research were obtained.

### CONFLICT OF INTEREST

The author of this work declares that he has no conflicts of interest.

#### REFERENCES

- N. S. Kardashev, A. V. Alakoz, A. S. Andrianov, M. I. Artyukhov, et al., Vestn. NPO Lavochkina, No. 3 (33), 4 (2016).
- C. R. Gwinn, M. V. Popov, N. Bartel, A. S. Andrianov, et al., Astrophys. J. 822, 96 (2016).
- 3. M. V. Popov, N. Bartel, C. R. Gwinn, M. D. Johnson, et al., Mon. Not. R. Astron. Soc. **465**, 978 (2017).
- M. V. Popov, A. S. Andrianov, M. S. Burgin, V. A. Zuga, A. G. Rudnitskii, T. V. Smirnova, V. A. Soglasnov, and E. N. Fadeev, Astron. Rep. 63, 391 (2019).
- T. V. Smirnova, V. I. Shishov, A. S. Andrianov, M. S. Burgin, et al., Mon. Not. R. Astron. Soc. 496, 5149 (2020).
- S. F. Likhachev, V. I. Kostenko, I. A. Girin, A. S. Andrianov, A. G. Rudnitskiy, and V. E. Zharov, J. Astron. Instrum. 6, 1750004-131 (2017).
- N. Bartel, M. S. Burgin, E. N. Fadeev, M. V. Popov, N. Ronaghikhameneh, T. V. Smirnova, and V. A. Soglasnov, Astrophys. J. 941, 112 (2022).
- 8. M. V. Popov, N. Bartel, M. S. Burgin, T. V. Smirnova, and V. A. Soglasnov, Mon. Not. R. Astron. Soc. **506**, 4101 (2021).
- 9. M. V. Popov, N. Bartel, C. R. Gwinn, M. D. Johnson, et al., Mon. Not. R. Astron. Soc. **465**, 978 (2017).
- 10. C. R. Gwinn, J. M. Cordes, N. Bartel, A. Wolszczan, and R. L. Mutel, Astrophys. J. **334**, L13 (1988).
- 11. A. T. Deller, W. M. Goss, W. F. Brisken, S. Chatterjee, et al., Astrophys. J. **875**, 100 (2019).

- 12. A. J. R. Prentice and D. Ter Haar, Mon. Not. R. Astron. Soc. **146**, 423 (1969).
- 13. M. Renzo and Y. Götberg, Astrophys. J. **923**, 277 (2021).
- 14. A. Blaauw, in *Massive Stars: Their Lives in the Interstellar Medium*, Ed. by J. P. Cassinelli and E. B. Churchwell, ASP Conf. Ser. **35**, 207 (1993).
- A. J. M. Thomson, T. L. Landecker, J. M. Dickey, N. M. McClure-Griffiths, et al., Mon. Not. R. Astron. Soc. 487, 4751 (2019).
- 16. A. V. Pynzar', Astron. Rep. 62, 123 (2018).
- 17. A. W. Clegg, A. L. Fey, and T. J. W. Lazio, Astrophys. J. **496**, 253 (1998).

- 18. Ue-Li Pen and Y. Levin, Mon. Not. R. Astron. Soc. **442**, 3338 (2014).
- Siqi Liu, Ue-Li Pen, J. P. Macquart, W. Brisken, and A. Deller, Mon. Not. R. Astron. Soc. 458, 1289 (2016).
- 20. C. R. Gwinn, N. Bartel, and J. M. Cordes, Astrophys. J. **410**, 673 (1993).

**Publisher's Note.** Pleiades Publishing remains neutral with regard to jurisdictional claims in published maps and institutional affiliations.

AI tools may have been used in the translation or editing of this article.